

Nanoengineered Light-Activatable Polybubbles for On-Demand Therapeutic Delivery

Shreedevi Arun Kumar, Jacob Good, David Hendrix, Eunsoo Yoo, Dongin Kim, Kaivalya A. Deo, Yong-Yu Jhan, Akhilesh K. Gaharwar,* and Corey J. Bishop*

Vaccine coverage is severely limited in developing countries due to inefficient protection of vaccine functionality as well as lack of patient compliance to receive the additional booster doses. Thus, there is an urgent need to design a thermostable vaccine delivery platform that also enables release of the bolus after predetermined time. Here, the formation of injectable and light-activatable polybubbles for vaccine delivery is reported. In vitro studies show that polybubbles enable delayed burst release, irrespective of cargo types, namely small molecule and antigen. The extracorporeal activation of polybubbles is achieved by incorporating near-infrared (NIR)-sensitive gold nanorods (AuNRs). Interestingly, light-activatable polybubbles can be used for on-demand burst release of cargo. In vitro, ex vivo, and in vivo studies demonstrate successful activation of AuNR-loaded polybubbles. Overall, the light-activatable polybubble technology can be used for on-demand delivery of various therapeutics including small molecule drugs, immunologically relevant protein, peptide antigens, and nucleic acids.

leads to incomplete scheduling of booster shots.^[2] Second, timing of the booster shots is often not closely followed leading to reduced efficacy of vaccines. Last, breaks in the cold-chain transport result in limited stability and functionality of the vaccines. There is thus an urgent need for single injection vaccines (SIV) that can preserve vaccine functionality and deliver multiple boluses at predefined times.^[3] This strategy reduces the need for multiple injections, thus improving vaccine coverage, while also potentially improving therapeutic efficacy. However, SIVs have not yet been commercialized due to challenges including antigen instability and inconsistent release kinetics.

Controlled cargo release has been achieved in the past using various organic and inorganic micro- and nanoparticles.

1. Introduction

Infectious diseases results in 1.5 million child mortality each year globally due to inadequate vaccine coverage.^[1] Limited vaccine coverage is attributed to multiple challenges in administration and storage of vaccines especially in the context of developing countries. First, limited access to medical facilities

However, these techniques often facilitate release profile that are limited to sustained or burst release profile depending on the delivery system. For example, inorganic carriers including silicate-based nanoparticles have multiple cargo pockets that results in sustained short-term release of the cargo (hours to days).^[4] These particles would potentially not be ideal for vaccine delivery that need burst release after specific durations. In the context, organic carriers obtained from emulsion-based systems are often used where cargo is exposed to organic and aqueous solvents, which result in limited cargo versatility.^[3a,5] Protein-based cargo, in particular, is exposed to damaging conditions during emulsification process leading to protein denaturation and instability.^[6] Other approaches have reduced solvent exposure through various modifications, but lack consistency in release kinetics.^[5b] For example, polyester-based microparticles were fabricated using StampED assembly of polymer layers (SEAL). Although this SIV technology enabled delayed pulsatile release, there are several limitations including cargo filling process of the SEAL technology which can then cause skewed filling alignment. This results in premature release of the cargo.


To overcome these limitations, we introduce a polybubble technology as an SIV platform by limiting solvent exposure, while accurately achieving predefined as well as on-demand release kinetics. Our polyester-based polybubble is an injectable platform with UV-cured polymer shell covering the centered cargo. Unlike other core-shell particles that are fabricated using emulsion-based methods, cargo within our polybubbles are exposed to significantly less organic solvent and thus can

S. Arun Kumar, J. Good, D. Hendrix, K. A. Deo, Y.-Y. Jhan, Prof. A. K. Gaharwar, Dr. C. J. Bishop
Biomedical Engineering
College of Engineering
Texas A&M University
College Station, TX 77843, USA
E-mail: gaharwar@tamu.edu; coreybishop@tamu.edu

Dr. E. Yoo, Prof. D. Kim
Irma Lerma Rangel College of Pharmacy
Texas A&M Health Science Center
Kingsville, TX 78363, USA

Prof. A. K. Gaharwar
Material Science and Engineering
College of Engineering
Texas A&M University
College Station, TX 77843, USA

Prof. A. K. Gaharwar
Center for Remote Health Technologies and Systems
Texas A&M University
College Station, TX 77843, USA

 The ORCID identification number(s) for the author(s) of this article can be found under <https://doi.org/10.1002/adfm.202003579>.

DOI: 10.1002/adfm.202003579

potentially preserve cargo stability. This polybubble platform can also enable delayed burst release profile that are particularly useful for vaccine applications while emulsion-based particles often enable continuous sustained release. On-demand delivery of cargo can also be achieved using our polybubble platform by incorporating light-responsive gold nanorods (AuNR) within the polybubble. These light-responsive polybubbles can be actuated upon near-infrared (NIR) exposure, which can penetrate few centimeters through the skin.^[7] In addition, photoacoustic imaging can be used to enable tracking of these nanoengineered polybubbles after injection.^[8] In this paper, cargo versatility of the polybubbles and delayed release of cargo from non-light-activatable polybubbles are characterized. In vitro, ex vivo and in vivo ability of these polybubbles to be light activated and in vitro and ex vivo studies for on-demand delivery of loaded cargo from the polybubbles are also evaluated. It is expected that the polybubble technology can be used for on-demand delivery of various therapeutics including small molecules drugs, antigens, proteins, peptides, and nucleic acids.

2. Results and Discussion

2.1. Formation and Characterization of Polybubbles

Polybubbles were fabricated using a phase-separation approach, where cargo dissolved in aqueous phase was injected into the polymer “bubbles” in organic phase (Figure 1a). Subsequently the polybubble is cured to obtain a solid polybubble (see experimental section for details). We used two different types of polymers—polycaprolactone (PCL) and poly(lactic-co-glycolic acid) (PLGA) to form polybubbles. PLGA diacrylate (PLGADA) was commercially purchased to form PLGA polybubbles whereas PCL triacrylate (PCLTA) was synthesized in house to form PCL polybubbles. Endcapping of PCL with the triacrylate groups was confirmed using nuclear magnetic resonance (Figure 1b). PCL and PLGA were selected due to their similar mechanical stability, biocompatibility, and tunable degradation profile. Size of the cured polybubbles was measured using the scanning electron microscope (SEM) images and was found to be 900 μm in diameter (Figure 1c). This size could potentially be optimized further using an automated platform to enable systemic injection. Polybubbles were manually cut in half using a razor to confirm the nonhollow interior of the cured polybubbles. The cytocompatibility of the PLGA polybubbles was studied by determining metabolic activity of human ovarian carcinoma cells (SKOV3) over multiple time points (day 5, 10, 15, and 25) (Figure 1d). No significant difference (t-test, $*p < 0.05$) was observed between the groups (polybubble and control) indicating that there is no cytotoxicity associated with the polybubbles and the fabrication approach.

Upon ensuring the cytocompatibility of the polybubbles, aqueous cargo was injected into the polybubbles and subsequently subjected to UV curing. Polybubbles with centered cargo limits the exposure to organic solvent that is typically observed in core shell particles formed using emulsion-based methods. By direct injection of cargo in center of polybubbles, issues related to sealing can also be avoided.^[3a] It is also crucial to have spherical polybubbles to ensure consistent laser

activation and release of cargo from the polybubbles. However, cargo centering and maintaining the sphericity of polybubbles proved to be challenging. Cargo had the propensity to move upwards toward the surface of the polybubble while the polybubble sunk to the bottom of vial when formed in water (Figure 1e). To maintain the sphericity of the polybubbles, viscosity of the aqueous solution, into which polymer is typically injected, was optimized using 10% (wt/vol) carboxymethyl cellulose (CMC). Viscosities of the cargo and the polymer were modified to enable cargo centering within the polybubbles. Specifically, the viscosity of the cargo was increased by mixing the cargo in 5% (wt/vol) CMC and the viscosity of PCL was modulated using potassium carbonate (K_2CO_3) that was isolated after PCLTA synthesis. Rheology study indicated that increasing K_2CO_3 concentration increased the dynamic viscosity of PCL which in turn enabled cargo centering in PCL polybubbles (Figure 1f). PCL polybubble mixed with 60 mg mL^{-1} of K_2CO_3 had dynamic viscosity of 0.7 Pa s. When the cargo was injected into this polybubble, cargo had the propensity to stay in the middle. Cargo centering was further confirmed by cutting the polybubble in half using a razor blade and visualizing using SEM (Figure 1g). Increase in viscosities is likely due to the generation of ionic species upon dissolution of CMC in water and reaction of K_2CO_3 with PCL as a proton scavenger during the endcapping reaction of PCLTA.^[9] To ensure that the reacted K_2CO_3 that was mixed with PCL does not negatively interfere with the therapeutic efficacy of the cargo, cytotoxicity studies were conducted in SKOV3 cells using a chemotherapy drug, doxorubicin (DOX), as a cargo. DOX mixed with reacted and unreacted 60 mg mL^{-1} K_2CO_3 were administered to SKOV3 cells and these groups were compared to control group that was treated with only DOX. When 1000×10^{-9} M DOX was used to treat SKOV3 cells, DOX mixed with reacted K_2CO_3 showed reduced SKOV3 viability of $25.7 \pm 3\%$, similar to that of the control group (no statistical difference between the groups). In contrast, DOX with unreacted K_2CO_3 showed increased SKOV3 viability of $68.7 \pm 8\%$. These results validated that the use of reacted K_2CO_3 maintained the therapeutic efficacy of DOX while also increasing the viscosity of PCL. Unlike PCL polybubbles, cargo centering in PLGA polybubbles did not require modulation of PLGA viscosity using K_2CO_3 . Similar to PCL polybubbles, PLGA polybubbles were formed in 10% (wt/vol) CMC solution and cargo mixed with 5% (wt/vol) CMC was injected in the middle. Similar to PCL polybubbles, centering of the cargo within PLGA polybubbles were confirmed using SEM images of cut polybubbles.

2.2. Delayed Burst Release from PCL and PLGA Polybubbles

After successful cargo centering within the PCL polybubbles, release studies were conducted. PCL polybubbles were loaded with a small molecule, acriflavine, and subjected to accelerated release conditions (50 °C and 70 °C) to assess the release kinetics. Delayed burst releases peaked on day 170 from polybubbles incubated at 50 °C and on day 58 from polybubbles incubated at 70 °C (Figure 2a,b). Although accelerated release studies showed delayed burst release of cargo in PCL polybubbles, burst release at physiological temperature would

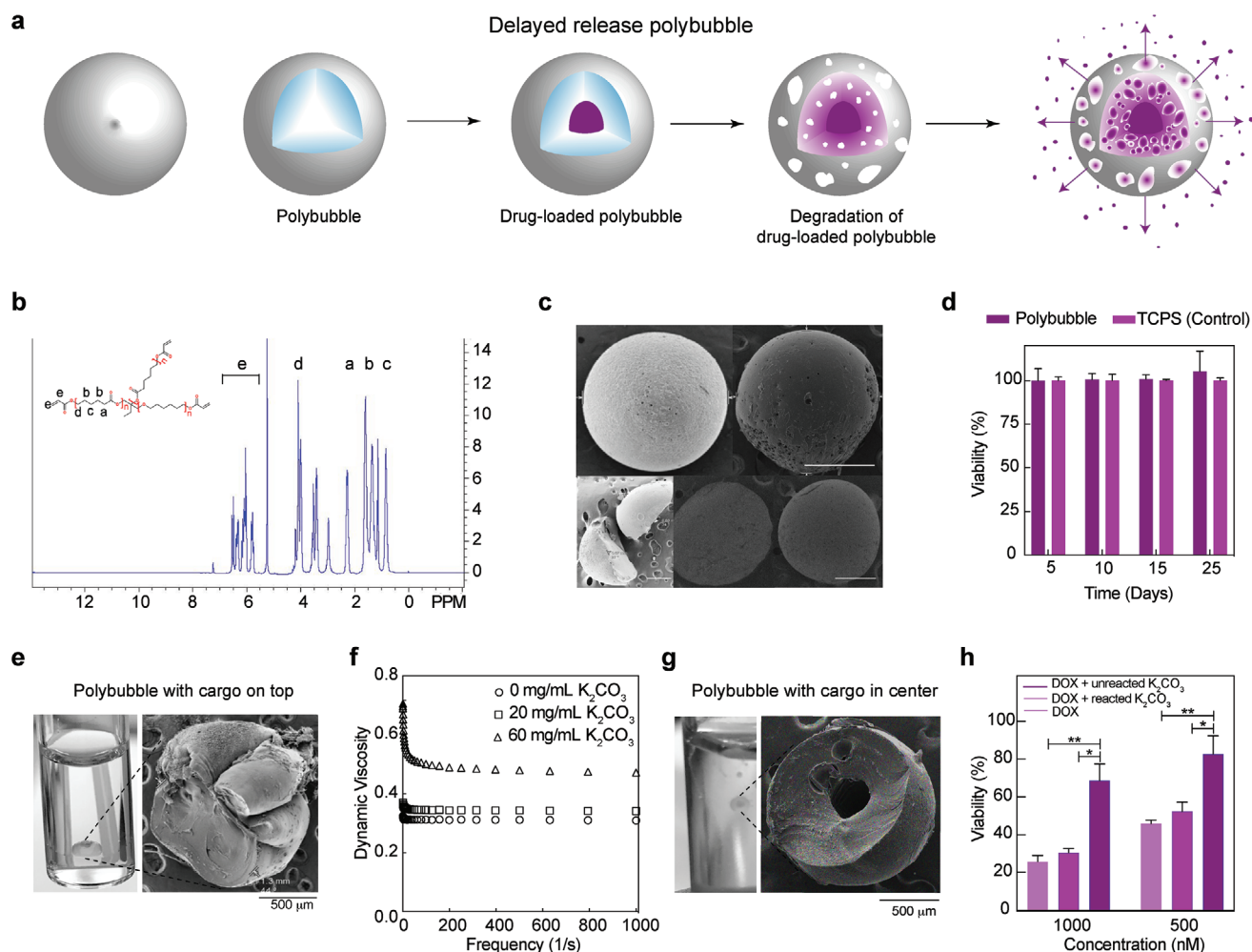


Figure 1. Formation and characterization of delayed-burst enabling polybubbles. a) Cured polyester-based polybubbles with centered cargo undergoing bulk erosion causing burst release of the cargo. b) NMR characterization of PCL that was endcapped with triacrylate groups (peaks labeled as e). c) SEM images of whole and cut PCL and PLGA polybubbles. Scale bars = 500 μm . d) In vitro study of SKOV3 cells incubated with PLGA polybubbles for 5, 10, 15, and 25 d shows that no cytotoxicity is caused by PLGA polybubbles. Centering of cargo within the PCL polybubbles were optimized by e) modulating the viscosity of the polymer using K_2CO_3 that was isolated after PCLTA endcapping reaction and g) modulating viscosity of the cargo using CMC. f) Cargo without CMC was injected into the polybubble causing the cargo to move towards to the surface of the polybubble. g) Cargo with 5% CMC was injected into the polybubble causing the cargo to be retained within the polybubble. h) In vitro study of SKOV3 cells treated with $1000 \times 10^{-9} \text{ M}$ and $500 \times 10^{-9} \text{ M}$ DOX and unreacted K_2CO_3 , DOX with reacted K_2CO_3 , and DOX shows that unreacted K_2CO_3 significantly reduced the therapeutic efficacy of DOX compared to reacted K_2CO_3 . ** $p < 0.01$, * $p < 0.05$, one-way ANOVA.

likely be delayed further (1–2 years).^[10] For vaccine applications that require booster shots to be administered periodically, polymers like PCL with slow degradation rate would be highly desirable. However, vaccines that require shorter intervals between doses and various other biomedical applications including delivery of synergistic chemotherapeutic agents could benefit from polymers that have high degradation rate. PLGA is one such polymer that is known to have faster degradation rate compared to PCL.^[11] As expected, delayed burst release of the cargo from PLGA polybubbles was observed much earlier when compared to that of PCL polybubbles. Delayed burst release peaked on day 16 from PLGA polybubbles that were incubated at 37 °C and on day 4 from PLGA polybubbles incubated at accelerated release condition (50 °C).

Cargo versatility of the polybubbles was also tested by assessing the release profiles of protein. Release studies were conducted with fluorescently labeled protein, BSA-488, as the centered cargo. In PCL polybubbles, release studies were conducted at 37 °C and at 50 °C and not at 70 °C because the cargo type is antigen which is highly sensitive to temperature. Delayed burst release peaked on days 58 and 90 from PCL polybubbles that were incubated at 37 °C. For PCL polybubbles that were incubated at 50 °C, release was continuous and did not indicate delayed release trend (Figure 2a,b). This difference is likely due to the effect of higher temperature on the antigen. Denaturation and breaking down of the antigen could potentially have caused the fluorophore detachment from the antigen and escape through the pores at higher temperatures. Release studies of PLGA polybubbles with BSA-488 as

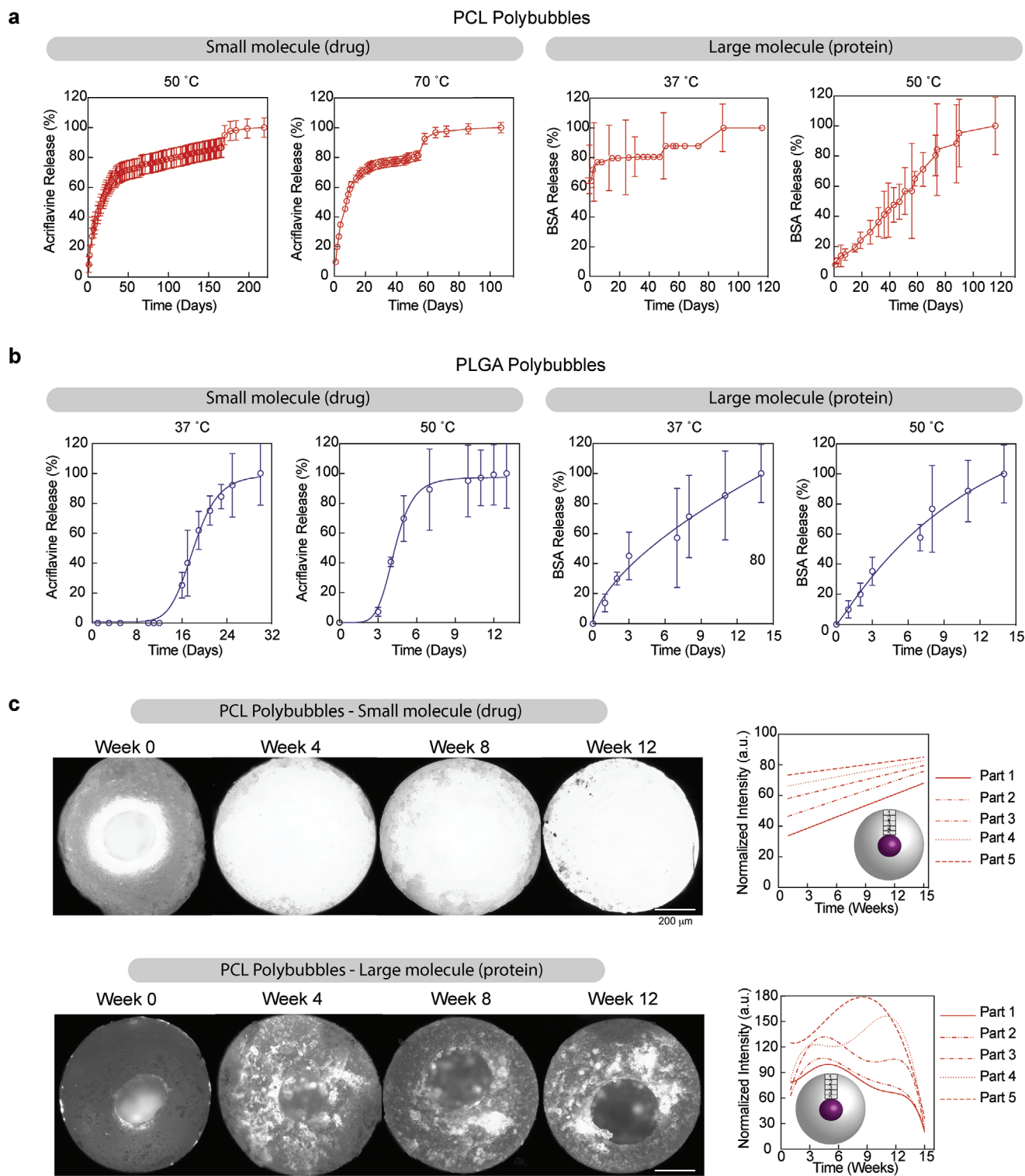


Figure 2. Delayed-burst release from polybubbles. a) Delayed burst release of acriflavine at 37 °C (day 16) and 50 °C (day 4) and release of BSA-488 from PLGA polybubbles at 37 °C (day 21) and 50 °C (day 7). b) Delayed burst release of acriflavine from PCL polybubbles at accelerated degradation conditions 50 °C (day 170) and 70 °C (day 58) and release of BSA-488 from PCL polybubbles at 37 °C (days 58 and 90) and 50 °C. Release of acriflavine was not observed at 37 °C owing to the long degradation rate of PCL polybubbles. c) Quantification of diffusion of acriflavine and BSA 488 through the wall of PCL polybubbles. Difference in diffusion pattern of acriflavine and BSA-488 potentially causes the difference in the release profiles of acriflavine and BSA-488 that are observed in 2a and 2b. Scale bars = 200 μ m.

the centered cargo were also conducted at 37 °C and at 50 °C. Delayed burst releases peaked on day 21 and day 7 for release studies conducted using polybubbles that were incubated at 37 °C and 50 °C, respectively. Although delayed burst releases were observed in PCL and PLGA polybubbles with different cargo types in the center, timing of cargo release is observed to be different. This difference in release profiles in the two cargo types is likely due to the size of the cargo and its mobility through the pores. Small molecules like acriflavine tend to diffuse through smaller pores resulting in an initial burst release effect seen in PCL polybubbles while large molecules like BSA-488 requires large interconnected pores to diffuse through the polymer shell. It is thus crucial to study the diffusion kinetics of different cargo types to accurately predict the release profile from the polybubbles.

2.3. Diffusion of Different Cargo Types and Porosity of Polybubbles

Polyester-based polybubbles (PCL or PLGA) are expected to show similar diffusivity trend as all the polyesters typically go through bulk erosion. PCL polybubbles with acriflavine or BSA-488 as centered cargo were incubated for predefined time points (1–15 weeks) (Figure S1, Supporting Information). At each time point, polybubbles were cut in half and the drug distribution was quantified by measuring the fluorescence in the polybubbles (Figure 2c). Diffusion through the polymer shell was assessed by dividing the shell into five parts (1st—center and 5th periphery). Small molecules uniformly diffused through the polymer wall resulting in uniform release of cargo over time. In contrast, relatively larger cargo, BSA-488, exhibited nonuniform diffusion resulting in pockets of antigen being distributed throughout the polymer wall. As hypothesized earlier, this difference in diffusion pattern is likely to have resulted from both the cargo size and pore size within the polymer shell. Small molecules, like acriflavine, are more likely to diffuse through the smaller pores relatively easily compared to that of larger molecules, such as BSA-488. Diffusion trend is a crucial factor in predicting release of cargo and these results highlight the importance of understanding the diffusivity of various cargo types within the delivery platform.

Diffusion patterns, irrespective of the cargo type, are also heavily dependent on the polymer porosity. Polyesters like PCL and PLGA typically undergo bulk erosion that are characterized by volume loss caused by increasing number of pores within the particles. Unlike surface erosion, overall size of the particle remains constant until complete degradation. Thus, porosity of the polybubbles was analyzed to better understand the degradation profile of the polybubbles. Both PCL and PLGA polybubbles were used for this study because of the difference in the degradation time of the two polyesters. Pores in the polybubbles, that were cut in half for the diffusion study, were studied using confocal microscopy (Figures S2 and S3, Supporting Information) and SEM images. Number of pores on the outer surface and inner surface of the polybubble halves were quantified. In both PCL and PLGA polybubbles, the number of pores on the outer surface increased over time (Figure 3a,b). However, there was variability in the timeline during which the

number of pores increased in the PCL and PLGA polybubbles owing to different degradation profiles. PCL is a slow degrading polymer causing the pore numbers to increase at a slower rate compared to that of a fast degrading polymer like PLGA. Additionally, the number of pores on the inner side of the cut polybubble does not increase over time. In PCL polybubbles, the number of pores on the inner side stayed constant throughout the 15 weeks of study as the degradation rate of PCL was much slower (Figure 3a). In PLGA polybubbles, no pores were observed until the end stages of degradation on day 15. By this point most pores are connected throughout the shell enabling the cargo to be released. The presence of lesser number of pores on the inner side could be the result of the high-water content that the outer surface of the polybubble is exposed to compared to that of the polybubble core. Because the polybubbles are lyophilized after cargo injection, less humidity is expected to be trapped within the core. However, incubating the polybubbles in PBS exposes the outer surface of the polymer to water resulting in increased number of pores on the outer side of the polybubbles. It is also important to note that pore size increases with degradation as observed in the SEM morphology images of outer and inner surfaces of PLGA polybubbles (Figure S4, Supporting Information). This phenomenon of increasing pore size as it relates to degradation in bulk eroding materials has been extensively studied in previous studies.^[12] Water absorption by the polymer shell, induced by degradation, increases overtime resulting in larger pockets or voids being formed in the shell. Eventually the pores are connected causing the release of the cargo.

2.4. Laser Activation of Polybubbles and On-Demand Release

Our polybubble technology could further benefit the goal of improved vaccine coverage by facilitating increased control over the timing of release. Release kinetics are generally dependent on various factors including polymer type, molecular weight, monomer ratio, and cargo type. However, designing different polymer systems to cater various vaccine schedules is not efficient. Thus, we focused on incorporating “on-demand” delivery of cargo in our polybubble platform (Figure 4a). By activating the polybubbles after they are injected, the release of cargo can be modulated on a need basis. NIR light can penetrate the skin making it attractive for in vivo applications and thus we wanted to use NIR-sensitive agents during the polybubble formation.

AuNRs have been extensively studied for their ability to absorb NIR light further leading to heat activation. CTAB-stabilized AuNRs were synthesized and were phase-transferred from aqueous solution to organic solvent, chloroform, based on previously published protocol^[33] (Figure S5, Supporting Information). The AuNRs' transverse and longitudinal diameters were 13 ± 4 and 50 ± 14 nm, respectively (Figure 4b). Hydrophobized AuNRs were mixed with the polymer (PCL or PLGA) prior to polybubble formation thus localizing AuNRs in the polymer shell. Cargo was subsequently injected in the middle and the polybubbles were cured. Polybubbles were then incubated in PBS and were heat activated using NIR laser for 5 min. Timing of laser activation was determined to be 5 min after conducting a release study using different groups of PLGA polybubbles

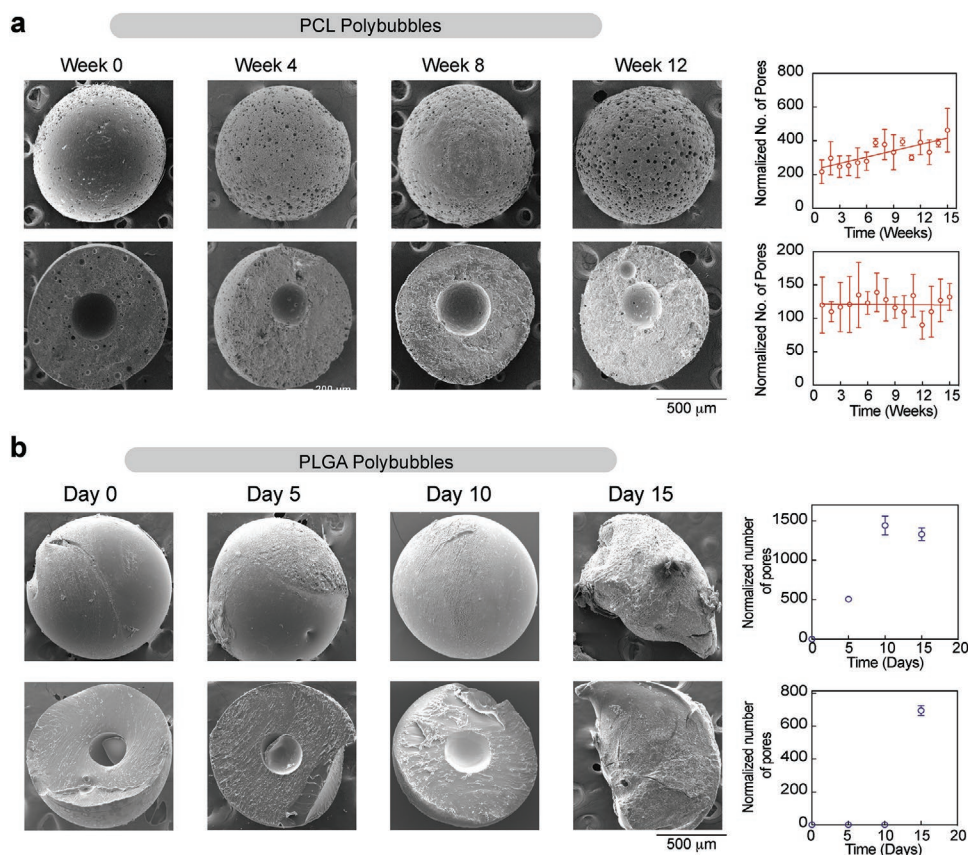


Figure 3. Degradation study of the polybubbles. a) Cut PCL polybubbles with increasing number of pores over 12 weeks on the outer surface and constant number of pores on the inner surface of PCL polybubbles. Number of pores increased on the surface of polybubble that was in direct contact with PBS during incubation while number of pores on the inner surface will only increase upon complete degradation of PCL. b) Cut PLGA polybubbles with increasing number of pores over 15 d on the outer and inner surface of PLGA polybubbles. Number of pores increase as PLGA degrades resulting in delayed release of cargo.

that were laser activated for 0, 5, 10, 15, and 20 min (Figure S6, Supporting Information). We then characterized the release kinetics of these polybubbles upon the incorporation of AuNRs. Release studies were conducted under the same conditions as described above in 2.2. The only variable that was altered was intermittent laser activation of the polybubbles. The supernatants were replaced with fresh PBS before the laser activation. Supernatants were collected after the 5 min of lasering and fluorescence was measured. This study showed that burst release occurred at earlier time points in both PCL and PLGA polybubbles compared to that of polybubbles without laser activation. For PCL polybubbles, burst release occurred on day 170 when incubated at 50 °C without laser activation while with laser activation the release was expedited to day 84 (Figure 4c). Similarly, for PLGA polybubbles, burst release peaked on day 19 when incubated at 37 °C while earlier burst release was observed to peak on day 7 from the polybubbles that were laser activated (Figure 4c). This study shows that there is a significant impact of AuNR-facilitated laser activation on the release kinetics of the cargo. Earlier release of cargo is likely due to the accelerated degradation of the polymer shell that is in turn caused by the increase in temperature. This feature of our polybubble platform thus has the potential to be clinically instrumental in the timely delivery of the cargo.

Another interesting observation was made during the laser activation release study regarding repeated exposure of polybubbles to the laser. The temperature change from before and after laser activation stayed relatively constant even after multiple laser sessions. For PCL and PLGA polybubbles, the temperature change observed to be 12 ± 1 °C and 11 ± 2 °C, respectively, and this change was maintained over time (Figure 5a). In previous studies, AuNRs have been known to lose their absorption efficiency after being laser activated multiple times.^[14] However, AuNRs retained their shape and thus maintained their absorption efficiency in our polybubble because AuNRs were entrapped within the rigid polymer shell. In addition to effective laser activation, validation of therapeutic efficacy of the cargo that is released upon laser activation is also crucial to ensure clinical success. PLGA polybubbles with centered DOX and AuNRs in the shell were incubated in cell culture media and were subjected to repeated NIR laser exposure. Supernatants were replaced with new media before and after each session of laser activation. Supernatants from both the groups, laser activated and nonlaser activated polybubbles, were delivered to SKOV3 cells. Average increase in temperature was observed to be 12 ± 1 °C and was maintained throughout the release study (Figure 5b). Release of DOX was quantified using fluorescence measurement of the collected supernatants.

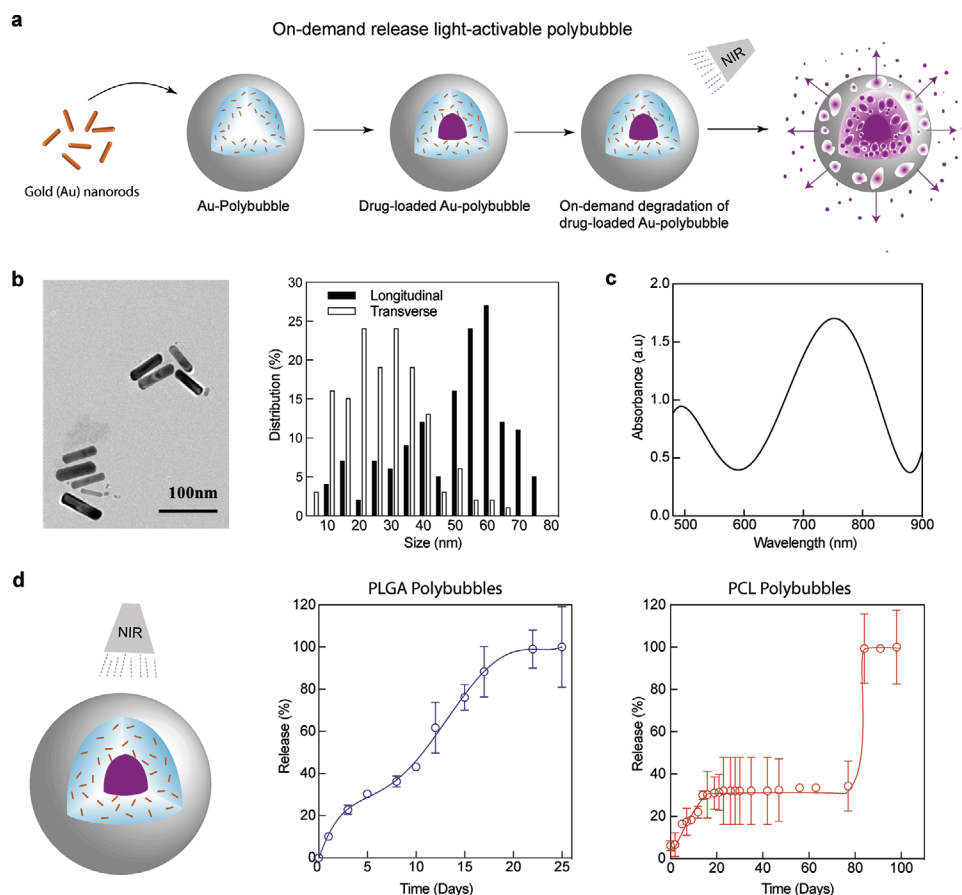


Figure 4. Characterization of gold nanorods (AuNRs) and laser-activated polybubbles. a) Polybubbles with AuNRs in the shell degrades faster upon multiple NIR laser activations. b) TEM images used for size characterization of longitudinal and transverse dimensions of synthesized AuNRs. c) Absorbance spectrum of AuNRs in the visible–NIR wavelength range. d) Expedited burst release from PLGA and PCL polybubbles (day 81) upon multiple periodic NIR laser activations.

Similar to the previous release studies, DOX release was expedited by 10 d in the laser group compared to the control group (Figure 5c). Reduction in cell viability was also significantly higher in cells that were treated with supernatants from laser-activated polybubbles compared to that of the control group on days 7 and 15 (Figure 5d). This reduction corresponds to the increased release of DOX from laser-activated polybubbles observed in Figure 5c. These results validate that therapeutic efficacy of cargo is in fact preserved after the release from the polybubbles upon laser activation.

2.5. In Vivo and Ex Vivo Laser Activation of Polybubbles

Upon successful laser activation of polybubble in vitro, we then tested in vivo efficacy of laser activation. We injected the PCL polybubbles with AuNRs in the shell into a melanoma tumor of balb-c white mice and observed the temperature differences from before and after laser activation (Figure 6a). There was a significant temperature increase of 8 ± 1 °C (t-test, $P < 0.0001$) after laser activation in mice that were injected with the AuNR-polybubbles compared to that of the control mice. Successful laser activation in vitro and in

vivo thus strengthens the prospect of translatability of this platform. After successful in vitro and in vivo laser activation studies, we wanted to assess the release kinetics of the cargo in physiological conditions. We thus carried out ex vivo laser-activated release study in bovine tissue. Release studies were carried out using PLGA polybubble with another centered small molecule, acriflavine. Polybubbles were laser activated for 5 min once every 2 d and the supernatants were replaced with fresh PBS. On day 11, the polybubbles were removed from the PBS and were placed between bovine cartilage and 1 cm of bovine meat (Figure 6b). Fluorescence images that were taken before and after laser activation showed that acriflavine was released into the surrounding cartilage upon laser activation. Quantification of the fluorescence images showed that fluorescence within the polybubble decreased from 98% to 30% after laser activation indicating the release of cargo (Figure 6g). In contrast, fluorescence of the cartilage increased from 2% to 70% after laser activation. This indicates that laser activation resulting in expedited cargo release can be successfully carried out ex vivo. The polybubble technology can thus potentially be activated extracorporeally using NIR laser to cater on-demand delivery of the cargo for various applications including in situ tissue regeneration, drug delivery, and additive manufacturing.^[15]

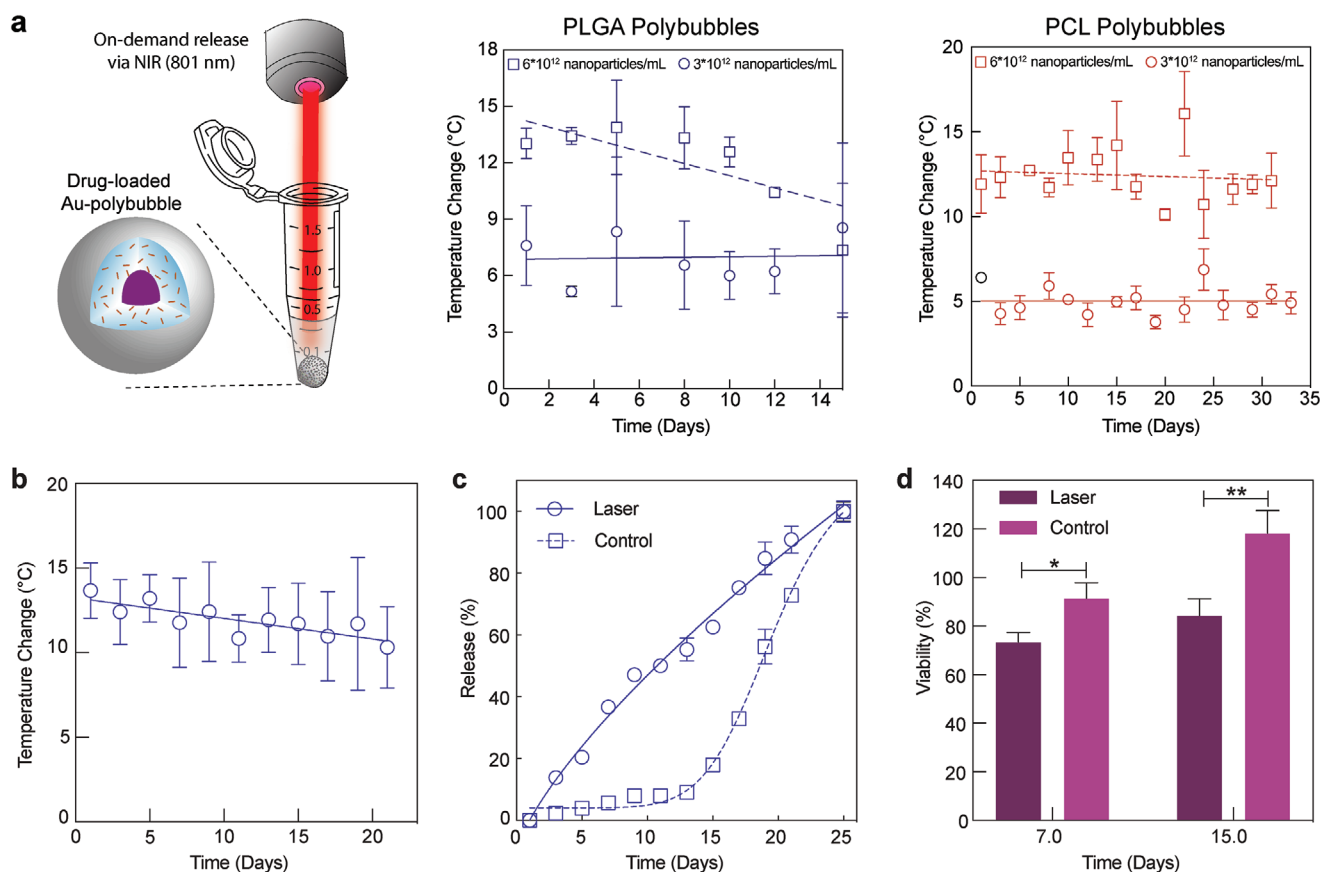


Figure 5. In vitro NIR-laser activation of polybubbles. a) In vitro activation of PLGA and PCL polybubbles using 801 nm laser resulting in temperature change of 11 ± 2 °C and 12 ± 1 °C, respectively. b) NIR laser activation of PLGA polybubbles with centered DOX resulting in 12 ± 1 °C. c) Expedited release of DOX from NIR-activated PLGA polybubbles by 10 d compared to that of the control group. d) Reduced viability of SKOV3 cells was observed when treated with DOX released from NIR-activated polybubbles compared to that of the control group ($n = 3$). * $p < 0.05$, ** $p < 0.01$, t-test.

3. Conclusions

We have successfully developed a polyester-based platform technology for controlling the release of cargo. Unlike other emulsion-based approaches, our technology comprises of a single large cargo pocket in the middle versus many small cargo pockets dispersed throughout the polymer shell, like in the case of micro/nanoparticles. This essentially minimizes the surface area of the cargo that is exposed to organic solvent. As a result, a variety of cargo types can be used including antigens, proteins, and peptides that are often sensitive to organic solvents. These polybubbles were further used to achieve novel delayed burst kinetics in both types of polyesters, PCL, and PLGA. Small and large molecule cargo were used to demonstrate delayed burst release from the polybubbles strengthening the claim about cargo compatibility. Release kinetics was also successfully modulated using NIR-activatable AuNRs. Multiple laser activations enabled the temperature of the polybubbles to be increased consistently by at least 13 °C in both PCL and PLGA polybubbles. Use of AuNRs further expedited the release of cargo in PCL polybubbles and in PLGA polybubbles in vitro and ex vivo. Overall, our theranostic-enabling delivery platform technology is based on biodegradable components that

can be used for controlled delivery of many therapeutic agents including small molecules, antigens, proteins, peptides, and nucleic acids.

4. Experimental Section

Materials: Acriflavine (Chem-Impex International), acryloyl chloride (Sigma Aldrich), ascorbic acid (Fisher Chemical), bovine serum albumin 488 (BSA-488) (Invitrogen), bromosalicylic acid (ACROS Organics), carboxymethylcellulose (CMC) (Alfa Aesar), centrionium bromide (CTAB), chloroform (Fisher Scientific), chlorauric acid (Fisher Scientific), dichloromethane (DCM) (ACROS Organics), diethyl ether (Fisher Chemical), doxorubicin hydrochloride (Fisher Scientific), 2-hydroxy-4'-(2-hydroxyethoxy)-2-methylpropylphenone (photoinitiator) (Sigma Aldrich), mPEG thiol (Laysan Bio), phosphate saline buffer (PBS) (Gibco), polycaprolactone (14 kDa; Sigma Aldrich), polycaprolactone triol (300 Da) (ACROS Organics), poly (lactic-co-glycolic acid) diacrylate (5 kDa) (CMTec), potassium carbonate (K_2CO_3) (ACROS Organics), silver nitrate (Fisher Chemical), sodium borohydride (Fisher Chemical), and triethyl amine (ACROS Organics) were taken.

Methods: Polymer for Polybubble Shell: Two types of polyesters were used, namely, PCL and PLGA. For the formation of PCL polybubbles, 1000 mg mL⁻¹ of 14 kDa PCL and synthesized 300 Da PCL triacrylate (PCLTA) were mixture in a 1:3 (vol/vol). PCL is known to have a slower degradation rate and thus mixture of noncrosslinked and

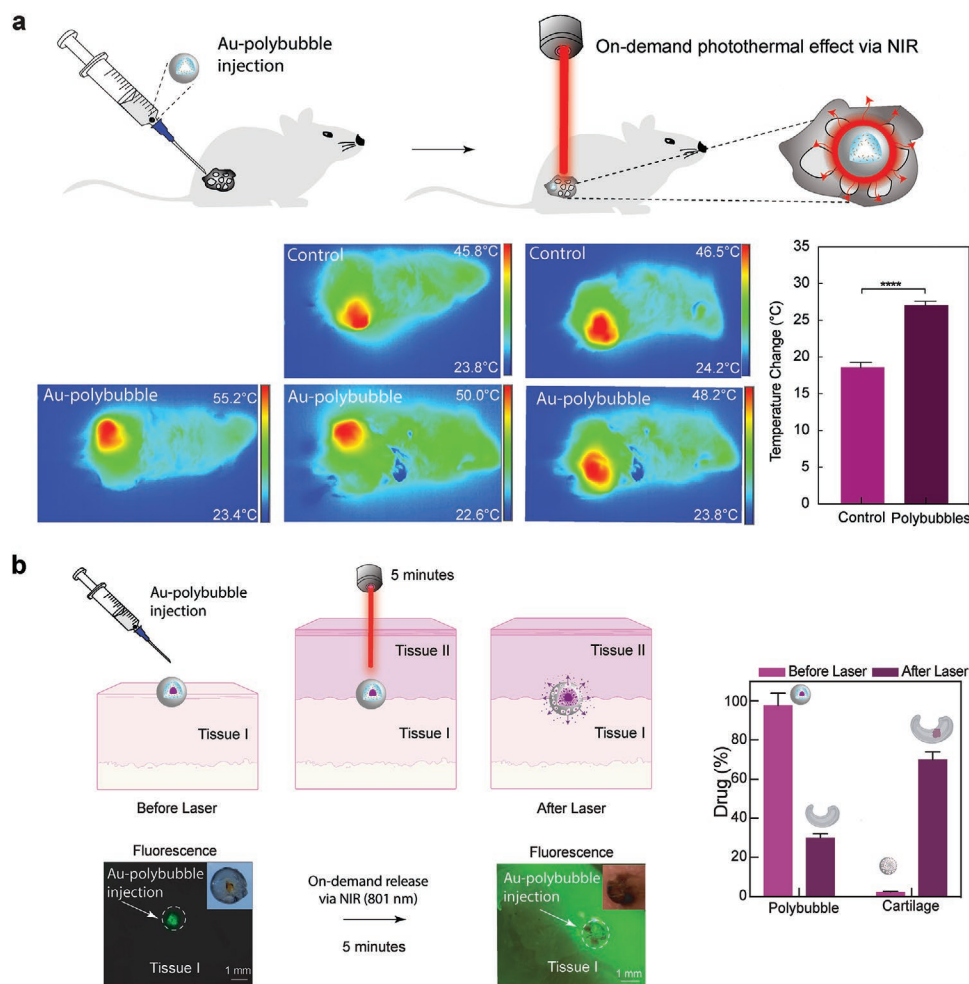


Figure 6. In vivo and ex vivo laser activation of polybubbles. a) In vivo laser activation of AuNR-polybubbles upon injection into melanoma tumor of Balb-C mice. Temperature increase of 8 ± 1 °C was observed after in vivo NIR laser activation of AuNR-polybubbles ($n = 3$). **** $p < 0.0001$, t-test. b) Ex vivo release study of PLGA polybubble with centered acriflavine. Acriflavine from PLGA polybubbles was released onto the cartilage (Tissue I) upon NIR laser activation ($n = 2$). ** $p < 0.01$, t-test. Scale bars = 1 mm.

crosslinked chains would be beneficial in increasing the degradation rate thus potentially leading to earlier cargo release. The synthesis, the quantification of PCLTA's viscosity, and quantification of PCLTA's absolute molecular weight were discussed. For PLGA polybubbles, 1200 mg mL⁻¹ of commercially purchased 5 kDa PLGADA was prepared in chloroform.

Polycaprolactone Triacrylate (PCLTA) Synthesis: In a round bottom flask, 3.2 mL of PCL triol was dried overnight at 50 °C under the low-pressure conditions using a water bath. Potassium carbonate (K₂CO₃) of mass 4.146 g was dried at 90 °C overnight. Twofold excess of dichloromethane (DCM) was used to dissolve PCL triol and dried K₂CO₃ was added to this mixture. Acryloyl chloride was measured based on the 1:3 molar ratio of PCL triol and acryloyl chloride. Acryloyl chloride was then dissolved in twofold excess of DCM and was added dropwise to the PCL triol and K₂CO₃. The reaction was carried out for 24 h under argon at room temperature and was filtered to remove excess K₂CO₃. The filtrate was then purified in threefold excess diethyl ether on a secondary container with ice. The purified PCLTA was then rotary evaporated to remove excess diethyl ether. The resultant oily PCLTA was then stored in the vacuum chamber overnight to remove residual diethyl ether.

Quantification of PCLTA Viscosity: PCLTA was mixed with various concentrations (0, 20, 60, 80 mg mL⁻¹) of reacted K₂CO₃ that was filtered after PCLTA synthesis. Anton Paar rheometer was used to change shear

rate from 1 to 1000 1/s with 31 data points. Then dynamic viscosity was calculated using shear stress (Pa) and shear rate (1/s).

Quantification of Absolute Molecular Weight of PCLTA: Mercury system (300 Hz) was used to analyze the polymer composition of PCLTA. PCLTA was quantified via nuclear magnetic resonance (NMR; TYPE; Bruker) by dissolving 100 µL sample in 900 µL of deuterated (D)-chloroform. Then 700 µL of each of the solution was transferred to their respective NMR tubes. Distinct proton signals corresponding to vinyl (endgroup) protons were identified and number of repeating units were calculated using the formula: $n = ((\text{sum of CH}_2 \text{ proton integrals}) / \# \text{ of CH}_2 \text{ protons}) / (\text{integral per proton value})$. Molecular weight of the polymer was then calculated using the formula: $(\text{FW end groups}) + ((\text{FW repeating unit}) * (n))$.^[16]

Polybubble Formation, Solidification, and Lyophilization: Polybubble Formation: For further information about polybubble formation is given in ref. [17]. Excess K₂CO₃ that was filtered out during the PCLTA synthesis was mixed with PCLTA to yield concentration of 60 mg mL⁻¹ to increase the viscosity to assist in cargo centering. PCLTA and K₂CO₃ mixture was then mixed with commercially purchased non-acrylate PCL in a 3:1 volume ratio. Polybubble tube using stainless steel (O.D.: 0.508 mm, I.D.: 0.254 mm) or nitinol (O.D.: 0.4064 mm, I.D.: 0.01 mm, 5 feet)

Polybubble Formation, Solidification, and Lyophilization: Ultraviolet (UV)-Curing and Lyophilization of the Polybubble: To cure polymer

mixture, 200 μL of either PCL/PCLTA or PLGADA was titrated with 2 μL of photoinitiator. After polybubbles were formed in 10% CMC solution in a 4 dram glass vial, the polybubbles were exposed to UV for 60 s. Cured polybubbles were then flash frozen in liquid nitrogen for 30 s and were lyophilized overnight.

Cargo Used for Loading Polybubbles: Small Molecules: 150 μL of 500×10^{-6} M doxorubicin (DOX) was added to 100 μL of 5% CMC. This solution was then injected into the polybubble using a stainless-steel tube using a 33 G round wire (O.D.: 0.2032 mm, I.D.: 0.1016 mm). 10 mg mL^{-1} acriflavine was prepared in DI water as cargo stock solution and then 1 mg mL^{-1} acriflavine was prepared using the 10 mg mL^{-1} stock solution in 5% CMC solution (aqueous). For cargo in the shell, 10 mg mL^{-1} acriflavine was prepared in DMSO and 10% (v/v) acriflavine was mixed with the polymer solution.

Cargo Used for Loading Polybubbles: Protein–Dye Conjugate: 0.5 mg mL^{-1} of BSA-488 was injected in the middle of the polybubbles and release studies were carried out at 37 °C and 50 °C.

Cargo Used for Loading Polybubbles: Loading of Drug within the Polybubble: Syringe pump (KD Scientific) was used to inject the polybubbles at the rate of 0.5 $\mu\text{L}/\text{sec}$. 31 G needle was used manually inject 1 mg mL^{-1} acriflavine or 0.5 mg mL^{-1} BSA-488 in 5% CMC in the middle of the polybubble.

Centering of Drug within the Polybubble and Release Studies: Centering of Drug within the Polybubble: Viscosity of the polymer was modulated increasing the concentration of K_2CO_3 that was isolated after the synthesis of PCLTA. Viscosity of the cargo was modulated using 5% (w/v) CMC.

Centering of Drug within the Polybubble and Release Studies: Release Studies (PCL): Release studies of PCL polybubbles with cargo in the middle and in the shell were incubated in 400 μL of PBS at 37 °C. However, PCL is known to have a longer degradation time^[18] and thus accelerated degradation studies were conducted by increasing the incubation temperatures. Polybubbles were incubated at 50 °C, 70 °C, and 90 °C and supernatants were collected at the desired time points. Samples were then filled with 400 μL of fresh PBS. Fluorescence intensities of the cargo in the supernatants were later measured using Cytation 5 (Biotek). Fluorescence data were then compared to that of the calibration curve of the cargo to determine the amount of cargo released.

Characterization of Polybubbles in the Absence of AuNRs: Quantification of Melting Temperature of PCL Polybubble: Differential scanning calorimetry (DSC) (Q_{20} , TA Instruments) was used to quantify the melting temperature transition point (T_m). Between 5 and 10 mg of polymer sample was weighed in an aluminum pan (T_0 , TA Instruments) and the lid was secured using a standard crimper. To quantify the PCLTA polybubble, the heating cycle ramped up the temperature from -40 °C to 150 °C at 1 °C min^{-1} (the instrument was not capable of going below -40 °C and interested in quantifying the T_m).

Characterization of Polybubbles in the Absence of AuNRs: Release Studies: Polybubbles were incubated in 400 μL of PBS and supernatants were collected at various time points. Polybubbles were then incubated with fresh PBS. Tubes were secured with yellow cap lock to prevent evaporation of PBS.

Characterization of Polybubbles in the Absence of AuNRs: Quantification of Internal Drug Distribution: PCL polybubbles with cargo in the middle were incubated in PBS at 50 °C for time points ranging from week 1 to week 15. Polybubbles from each time point were removed from the supernatants and were cut in half using the razor blade. Halved polybubbles were then imaged using Zeiss fluorescent microscope. Fluorescence in the shell of the polybubble was quantified by equally dividing the top half of each polybubble into five parts. Fluorescent intensities were quantified using ImageJ software.

Characterization of Polybubbles in the Absence of AuNRs: Quantification of Pore Formation: Polybubbles that were cut in half for assessing drug distribution were used for this study. The halved polybubbles were sputter coated with gold such that the outer surface of one half of the polybubble and the inner surface of the other half of the polybubble were coated. SEM images of the polybubbles from each time point (every

week from week 1 to week 15) were taken using the FEI Quanta 600 and triplicates were used for each time point. The SEM images were then converted to black and white images in ImageJ such that the pores were black. Then the pore sizes were measured using the circularity constraint in ImageJ. Number of pores along with the standard deviation were then determined for each time point.

AuNR Synthesis, Hydrophobization, and Characterization: AuNR Synthesis: 420 μL of seed solution (as follows) was added to the growth solution (as follows) which was left to react for 16 h. Excess CTAB was then removed by centrifuging for 30 min at 8k relative centrifugal force (RCF). The AuNR seed solution was made by mixing 250 μL of 10×10^{-3} M HAuCl_4 , 7.5 mL of 100×10^{-3} M CTAB, and 600 μL of 10×10^{-3} M ice cold NaBH_4 to a tube. The contents were then mixed for 2 min. The AuNR growth solution was made by thoroughly mixing 40 mL of 100×10^{-3} M CTAB, 1.7 mL of 10×10^{-3} M HAuCl_4 , 250 μL of AgNO_3 , and 270 μL of 17.6 mg mL^{-1} ascorbic acid to a tube.

AuNR Synthesis, Hydrophobization, and Characterization: Hydrophobization of AuNRs: Two different methods were used for hydrophobizing AuNRs. The first entailed toluene, and the second entailed chloroform. In the toluene-based approach, 2 mL of AuNRs was added to a scintillation vial and added 0.102 mL of undecanethiol to the vial. For every 2.102 mL of AuNR and undecanethiol, 0.51 mL of acetone and toluene was added. Added another 0.51 mL of acetone. This was spun in multistir plate for a few seconds. Pipetted out the top layer of organic phase and stored it in a separate scintillation vial. Repeated the addition of acetone and toluene steps and separation of organic phase until the aqueous phase is cloudy and colorless and the organic phase is clear.^[19] For the chloroform-based approach, the pH of 5.1×10^{-9} M of CTAB-stabilized AuNRs was adjusted to 10 using 1×10^{-3} M NaOH and AuNRs were stirred with 0.3×10^{-3} M mPEG thiol at 400 RPM overnight.^[13] 0.4 M of DDA was prepared in chloroform and was stirred with PEGylated AuNRs for 4 d at 1200 RPM.

AuNR Synthesis, Hydrophobization, and Characterization: AuNR Characterization: The AuNRs' transverse and longitudinal diameters using transmission electron microscopy (JEM-2010 TEM; JEOL) were used. A stock solution of AuNRs was placed for 30 s on the carbon-coated copper grid (10 nm thickness Formvar film grid; Electron Microscop Services) face to allow for AuNR adsorption with and without ethanol. Subsequently, the excess solution was blotted for removal. The concentrations of AuNRs were characterized using Cytation 5 (Biotek) assuming extinction coefficient of 2×10^9 L mol^{-1} cm^{-1} .^[20] Three wells of an acrylic 96-well plate were filled with 100 μL of filtered AuNRs. One well was filled with 100 μL of DI water to obtain the background absorbance. Then the spectral scanning absorbance setting was used to measure the absorbance of AuNRs between 300 and 900 nm with a step size of 1 nm.

Characterization of Polybubbles with Shell-Loaded AuNRs: AuNR and Polybubble Heating (In Vitro): Because near infrared (NIR) penetrates biological tissue on the order of a few centimeter,^[21] NIR wavelengths (801 nm) were used to heat polybubbles and using AuNRs which have surface plasmon resonance (SPR) wavelengths in the NIR, which enables them to heat. Polybubbles with AuNRs (in 400 μL PBS) were similarly heated for 5 min using the NIR laser with 13.4 watts (spot size of ≈ 1 cm) and temperature of both PCL and PLGA polybubbles before and after lasering was compared. An FTIR camera was used to record the temperature change during the lasering process.

Characterization of Polybubbles with Shell-Loaded AuNRs: Drug Release with Shell-Loaded AuNRs: Polybubbles with small molecule, acriflavine, in the middle and AuNRs in the shell were incubated at 37 °C for PLGADA polybubbles and at 50 °C for PCL/PCLTA polybubbles. Every Monday, Wednesday, and Friday, the polybubbles were laser activated for 5 min using the NIR laser at 801 nm and 8 A power. Supernatants were collected before laser activation and polybubbles were incubated with 400 μL of fresh PBS. To measure the amount of cargo released after laser activation, supernatants were collected again and fluorescence intensities were measured using Cytation 5 (Biotek, VT). Polybubbles were incubated with 400 μL of fresh PBS until the next laser activation time point.

In Vivo Work Involving the Thermo-therapy Capabilities of the Polybubble: Cell Culture for In Vivo Study: Melanoma (B16F10) cells, passage 5, were cultured in T175 flasks at 1×10^5 cells mL⁻¹ in RPMI-1640 medium with L-glutamine supplemented, 10% fetal bovine serum (FBS), and 2% penicillin streptomycin. B16F10 at a density of 5×10^6 cells were seeded in a T175 flask under standard conditions at 37 °C with 5% CO₂ and 100% humidity.

In Vivo Work Involving the Thermo-therapy Capabilities of the Polybubble: Subcutaneous (s.c.) Inoculation of Melanoma Cells and In Vivo Study: All the experimental protocols were approved by Texas A&M University Institutional Animal Care and Use Committee. To produce solid melanoma in the mice, BALB/c mice ($n = 6$) were inoculated with B16F10 cells via subcutaneous injection of 5×10^6 cells in 100 µL of PBS. After tumor inoculation, the tumor nodules were allowed to grow ≈ 50 to 100 mm³ for 2 weeks. One polybubble in 100 µL PBS was applied to the tumor via intratumoral injection. Immediately after the intratumoral injection, near infrared (NIR) laser light (Jenoptik Laser GmbH, Jenoptik, Germany) at 803 nm with 8 A applied to tumor area for 3 min. To validate the heat generation, the temperature of the exposed tumor with a microbubble and with PBS (without a polybubble) as a control was monitored by a thermal camera (FLIR-A300, FLIR Systems Inc., MA, USA) during the NIR irradiation.

In Vitro and Ex Vivo Work Involving On-Demand Release of Polybubbles upon Laser activation: Cell Culture for In Vitro Study: PLGA polybubbles with AuNRs in the shell were formed as described in 4.2.2 and 0.1 µL of 3 mg mL⁻¹ DOX was injected in the middle. Polybubbles were incubated in 200 µL McCoy's 5A media and were laser activated for 5 min using 8A of 801 nm NIR laser once every 2 d. Supernatants were collected after each laser activation and were replaced with fresh media. 100 µL of the supernatant was used to obtain fluorescence measurements using Cytation 5 (Biotek). SKOV3 cells were seeded in a 96-well plate (5000 cells per well) and 16 h after seeding, 100 µL of the supernatants from days 7 and 15 were delivered to SKOV3 cells.

In Vitro and Ex Vivo Work Involving On-Demand Release of Polybubbles upon Laser activation: Ex Vivo Study: PLGA polybubbles with AuNRs in the shell were formed as described in 4.2.2 and 0.1 µL of 1 mg mL⁻¹ acriflavine was injected in the middle. Polybubbles were incubated in 200 µL PBS and were laser activated for 5 min using 8A of 801 nm NIR laser once every 2 d. Supernatants were collected after each laser activation and were replaced with fresh PBS. On day 10, polybubbles were placed between a piece of bovine cartilage and 1 cm meat. Fluorescence images were obtained before laser activation. 8A of 801 nm NIR laser was used to activate the sandwiched polybubble for 5 min. Fluorescence images were then obtained after laser activation. Fluorescence intensities in the polybubbles and the cartilage were quantified using Image J analysis.

Statistical Analysis: All the statistical analyses were performed using GraphPad Prism software (GraphPad Software, La Jolla, CA, USA). Triplicates for each group were used for all the in vitro studies. Student's t-tests were conducted between the control and experimental groups in Figures 1d and 6d. Values were considered to be statistically significant if *p*-values were less than 0.05. One-way ANOVA was conducted between the three groups in Figure 1h. In the in vivo study conducted using laser-activated polybubbles, temperature change of the experimental group after laser activation are reported as average value from the independent triplicate values. For the control group, temperature change after laser activation is reported as average value from the technical triplicates. Temperature differences were analyzed using student's t-test and were considered statistically significant if *p*-values were less than 0.05.

Supporting Information

Supporting Information is available from the Wiley Online Library or from the author.

Acknowledgements

The authors acknowledge Dr. Changsun Kang from Dr. Dongin Kim's lab for help with NIR laser. C.J.B. thanks Texas A&M Engineering

Experimentation Station and the Department of Biomedical Engineering for providing funding. Use of the Texas A&M Microscopy and Imaging Center is acknowledged. The FE-SEM acquisition was supported in part by the National Science Foundation under Grant No. DBI-0116835. A.K.G. acknowledges financial support from the National Institute of Biomedical Imaging and Bioengineering (NIBIB) of the National Institutes of Health (NIH) Director's New Innovator Award (DP2 EB026265). The content is solely the responsibility of the authors and does not necessarily represent the official views of the funding agency.

Conflict of Interest

The authors declare no conflict of interest.

Keywords

delayed burst, diffusion, drug depot, light-activatable polybubbles, nanomaterials, stimuli responsive materials

Received: April 23, 2020

Published online:

- [1] M. Champeau, J. M. Thomassin, T. Tassaing, C. Jerome, *Expert Opin. Drug Delivery* **2017**, *14*, 1293.
- [2] S. Y. Tzeng, R. Guarecuco, K. J. McHugh, S. Rose, E. M. Rosenberg, Y. Zeng, R. Langer, A. Jaklenec, *J. Controlled Release* **2016**, *233*, 101.
- [3] a) K. J. McHugh, T. D. Nguyen, A. R. Linehan, D. Yang, A. M. Behrens, S. Rose, Z. L. Tochka, S. Y. Tzeng, J. J. Norman, A. C. Anselmo, X. Xu, S. Tomasic, M. A. Taylor, J. Lu, R. Guarecuco, R. Langer, A. Jaklenec, *Science* **2017**, *357*, 1138; b) K. J. McHugh, R. Guarecuco, R. Langer, A. Jaklenec, *J. Controlled Release* **2015**, *219*, 596; c) S. Y. Tzeng, K. J. McHugh, A. M. Behrens, S. Rose, J. L. Sugarman, S. Ferber, R. Langer, A. Jaklenec, *Proc. Natl. Acad. Sci. USA* **2018**, *115*, E5269.
- [4] a) Z. Z. Li, L. X. Wen, L. Shao, J. F. Chen, *J. Controlled Release* **2004**, *98*, 245; b) M. Vallet-Regi, M. Colilla, I. Izquierdo-Barba, M. Manzano, *Molecules* **2017**, *23*, E47; c) M. Bouchoucha, M.-F. Côté, R. C.-Gaudreault, M.-A. Fortin, F. Kleitz, *Chem. Mater.* **2016**, *28*, 4243; d) L. M. Cross, J. K. Carrow, X. Ding, K. A. Singh, A. K. Gaharwar, *ACS Appl. Mater. Interfaces* **2019**, *11*, 6741; e) A. K. Gaharwar, L. M. Cross, C. W. Peak, K. Gold, J. K. Carrow, A. Brokesh, K. A. Singh, *Adv. Mater.* **2019**, *31*, 1900332; f) C. W. Peak, K. A. Singh, M. a. Adlouni, J. Chen, A. K. Gaharwar, *Adv. Healthcare Mater.* **2019**, *8*, 1801553.
- [5] a) I. J. Joye, D. J. McClements, *Curr. Top. Med. Chem.* **2016**, *16*, 1026; b) D. Dutta, C. Fauer, K. Hickey, M. Salifu, S. E. Stabenfeldt, *J. Mater. Chem. B* **2017**, *5*, 4487; c) X. Yu, A. H. Biedrzycki, A. S. Khalil, D. Hess, J. M. Umhoefer, M. D. Markel, W. L. Murphy, *Adv. Mater.* **2017**, *29*, 1701255; d) K. Fu, A. M. Klibanov, R. Langer, *Nat. Biotechnol.* **2000**, *18*, 24; e) S. Frokjaer, D. E. Otzen, *Nat. Rev. Drug Discovery* **2005**, *4*, 298.
- [6] a) R. T. Bartus, M. A. Tracy, D. F. Emerich, S. E. Zale, *Science* **1998**, *281*, 1161; b) S. D. Putney, P. A. Burke, *Nat. Biotechnol.* **1998**, *16*, 153.
- [7] a) X. Huang, I. H. El-Sayed, W. Qian, M. A. El-Sayed, *J. Am. Chem. Soc.* **2006**, *128*, 2115; b) A. Wijaya, S. B. Schaffer, I. G. Pallares, K. Hamad-Schifferli, *ACS Nano* **2009**, *3*, 80.
- [8] a) S. Manohar, C. Ungureanu, T. G. Van Leeuwen, *Contrast Media Mol. Imaging* **2011**, *6*, 389; b) J. V. Jokerst, A. J. Cole, D. Van de Sompel, S. S. Gambhir, *ACS Nano* **2012**, *6*, 10366.
- [9] a) L. Cai, S. Wang, *Polymer* **2010**, *51*, 164; b) X. H. Yang, W. L. Zhu, *Cellulose* **2007**, *14*, 409.

- [10] Y. Hu, L. Zhang, Y. Cao, H. Ge, X. Jiang, C. Yang, *Biomacromolecules* **2004**, 5, 1756.
- [11] H. J. Sung, C. Meredith, C. Johnson, Z. S. Galis, *Biomaterials* **2004**, 25, 5735.
- [12] a) S. Lyu, D. Untereker, *Int. J. Mol. Sci.* **2009**, 10, 4033; b) L. Wu, J. Ding, *J. Biomed. Mater. Res. A* **2005**, 75, 767.
- [13] M. G. Soliman, B. Pelaz, W. J. Parak, P. del Pino, *Chem. Mater.* **2015**, 27, 990.
- [14] a) W. Albrecht, T. S. Deng, B. Goris, M. A. van Huis, S. Bals, A. van Blaaderen, *Nano Lett.* **2016**, 16, 1818; b) S.-S. Chang, C.-W. Shih, C.-D. Chen, W.-C. Lai, C. R. C. Wang, *Langmuir* **1999**, 15, 701; c) S. Link, C. Burda, M. B. Mohamed, B. Nikoobakht, M. A. El-Sayed, *J. Phys. Chem. A* **1999**, 103, 1165.
- [15] a) A. M. Brokesh, A. K. Gaharwar, *ACS Appl. Mater. Interfaces* **2020**, 12, 5319; b) H. P. Lee, A. K. Gaharwar, *Adv. Sci.* **2020**, <https://doi.org/10.1002/advs.202000863>; c) D. Chimene, R. Kaunas, A. K. Gaharwar, *Adv. Mater.* **2020**, 32, 1902026.
- [16] J. U. Izunobi, C. L. Higginbotham, *J. Chem. Educ.* **2011**, 88, 1098.
- [17] J. Lee, S. Arun Kumar, W. N. Souery, T. Hinsdale, K. C. Maitland, C. J. Bishop, *J. Biomed. Mater. Res. A* **2019**, 107, 2160.
- [18] M. S. Ibrahim, N. A. El-Wassefy, D. S. Farahat, in *Biomaterials for Oral and Dental Tissue Engineering*, (Eds: L. Tayebi, K. Moharamzadeh), Woodhead Publishing, Cambridge, England **2017**, p. 117.
- [19] S. Kittler, S. Hickey, T. Wolff, A. Eychmüller, *Zeitschrift für Physikalische Chemie* **2015**, 229, 235.
- [20] R. D. Near, S. C. Hayden, R. E. Hunter, D. Thackston, M. A. El-Sayed, *J. Phys. Chem. C* **2013**, 117, 23950.
- [21] T. A. Henderson, L. D. Morries, *Front Psychiatry* **2017**, 8, 187.